A Three-Dimensional in Silico Pharmacophore Model for Inhibition of *Plasmodium falciparum* Cyclin-Dependent Kinases and Discovery of Different Classes of Novel Pfmrk Specific Inhibitors†

Apurba K. Bhattacharjee,*,‡ Jeanne A. Geyer,‡ Cassandra L. Woodard,‡ April K. Kathcart,‡ Daniel A. Nichols,‡ Sean T. Prigge,§ Zhiyu Li,‡ Bryan T. Mott,‡ and Norman C. Waters*,‡

Division of Experimental Therapeutics, Walter Reed Army Institute of Research, Silver Spring, Maryland 20910-7500, and Department of Molecular Microbiology and Immunology, Malaria Research Institute, Johns Hopkins Bloomberg School of Public Health, Baltimore, Maryland 21205

Received June 1, 2004

The cell division cycle is regulated by a family of cyclin-dependent protein kinases (CDKs) that are functionally conserved among many eukaryotic species. The characterization of plasmodial CDKs has identified them as a leading antimalarial drug target in our laboratory. We have developed a three-dimensional QSAR pharmacophore model for inhibition of a *Plasmodium falciparum* CDK, known as Pfmrk, from a set of fifteen structurally diverse kinase inhibitors with a wide range of activity. The model was found to contain two hydrogen bond acceptor functions and two hydrophobic sites including one aromatic-ring hydrophobic site. Although the model was not developed from X-ray structural analysis of the known CDK2 structure, it is consistent with the structure−functional requirements for binding of the CDK inhibitors in the ATP binding pocket. Using the model as a template, a search of the in-house three-dimensional multiconformer database resulted in the discovery of sixteen potent Pfmrk inhibitors. The predicted inhibitory activities of some of these Pfmrk inhibitors from the molecular model agree exceptionally well with the experimental inhibitory values from the in vitro CDK assay.

Introduction

New chemotherapies to treat malaria are needed in light of the rapid development of drug resistance.[1,2] Malaria drug development efforts in the past have focused primarily on identifying compounds that inhibited the growth of the parasites in culture. With the completion of the *Plasmodium falciparum* genome project and the emergence of structure-based drug design methodologies, drug development efforts have shifted to targeting specific proteins in the parasite that are unique yet critical for cellular growth and survival. With a direct role in the regulation of cellular proliferation, the cyclin-dependent proteins kinases (CDKs) are attractive drug targets.[3,4]

CDKs have been identified as potential chemotherapeutic targets to treat a range of diseases to include cancer, cardiovascular and neurological disorders, and infectious disease.[5−8] A significant amount of CDK data from a variety of organisms has helped to initiate efforts to target the plasmodial CDKs. Sequence alignments, molecular models, and crystal structures of the plasmodial CDKs identified several amino acids within the active pocket that are different from mammalian CDKs.[9−11] Exploitation of these subtle differences can lead to potent and specific inhibitors. This has been demonstrated among the highly conserved mammalian CDKs in which minor active pocket differences were responsible for inhibitor specificity of CDK4/6 over CDK1/2.[4,12] Commercially available CDK inhibitors have a broad range of activity toward the plasmodial CDKs that reflects differences in active pocket binding.[13] Compounds have been identified that can discriminate among host and parasite CDKs. Woodard et al have shown that oxindole-based compounds are selective for the plasmodial CDK, Pfmrk, over other plasmodial CDKs and human CDK1.[11] Molecular models suggest that these compounds fit into the active site in the same orientation as they do in human CDK2; however, the compounds make additional contacts that are responsible for its specificity toward Pfmrk. Crystal structures of PfPK5 bound to inhibitors also demonstrate that inhibitors can bind to the ATP ribose phosphate binding site in a similar fashion as human CDKs, and amino acid differences adjacent to the ATP binding pocket site can be exploited for specific inhibitor design.[10]

Plasmodial CDK drug discovery efforts have used the amino acid sequence variations between the plasmodial and mammalian CDKs in an effort to identify selective inhibitors with high specificity.[13] The three plasmodial CDKs that are currently being investigated are PfPK5, PfPK6, and Pfmrk.[14] PfPK5 is most similar to human

* Corresponding authors. A.K.B. (computational and molecular modeling sections): Department of Medicinal Chemistry, Division of Experimental Therapeutics, Walter Reed Army Institute of Research, 503 Robert Grant Ave., Silver Spring, MD 20910; tel, 301-319-9043; fax, 301-319-9449; e-mail, apurba.bhattacharjee@na.amedd.army.mil. N.C.W. (biological section): Department of Parasitology, Division of Experimental Therapeutics, Walter Reed Army Institute of Research, 503 Robert Grant Ave., Silver Spring, MD 20910; tel, 301-319-9324; fax, 301-319-9449; e-mail: norman.waters@na.amedd.army.mil.

† Material has been reviewed by the Walter Reed Army Institute of Research. There is no objection to its presentation and/or publications. The opinions or assertions contained herein are the private views of the authors, and are not to be construed as official, or as reflecting true views of the Department of the Army or the Department of Defense.

‡ Walter Reed Army Institute of Research.

§ Johns Hopkins Bloomberg School of Public Health.

10.1021/jm040108f CCC: $27.50
Published on Web 09/25/2004

Chart 1

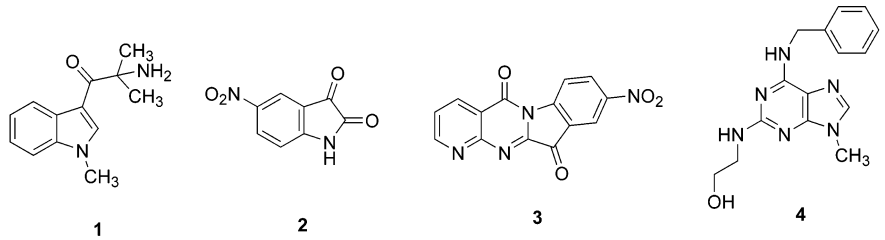

1 **2** **3** **4**

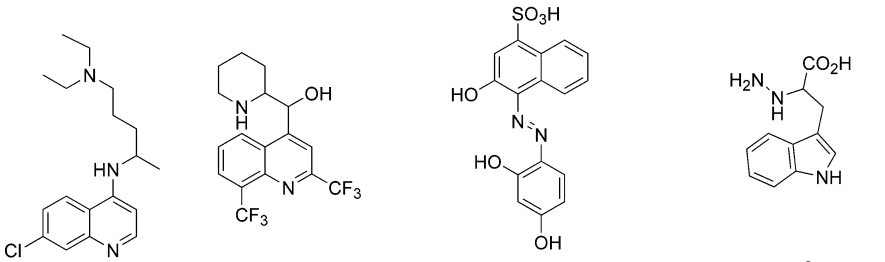

5 **6** **7** **8**

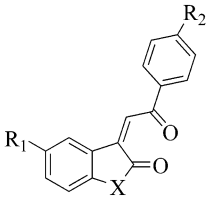

9: R_1 = H, R_2 = H, X = NH
10: R_1 = Br, R_2 = H, X = NH
11: R_1 = CH_3, R_2 = H, X = NH
12: R_1 = Br, R_2 = CH_3, X = NH
13: R_1 = H, R_2 = H, X = NCH_3

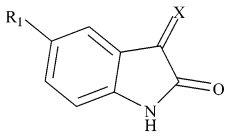

14: R_1 = NO_2, X = CH-phenol
15: R_1 = OCH_3, X = 2-thioxothiazolidin-4-one

CDK1 and is susceptible to many of the same inhibitors.[15,16] Several PfPK5 inhibitors are purine-based and include compounds such as olomoucine and purvalanol A. These same inhibitors possess antiparasitic activity when assayed with the malarial parasites in vitro, which suggests an essential role of CDKs in parasite growth and development.[17] Pfmrk shares the greatest sequence identity to human CDK7; however, many of the well-characterized CDK inhibitors presently available do not inhibit the activity of Pfmrk.[18,19] Novel amino acid sequence variations in the active site, homology with global CDK activation, and lack of inhibition by known CDK inhibitors make Pfmrk a promising CDK target in the parasite. Two separate classes of compounds, oxindoles and quinilinones, have been identified as significant inhibitors of Pfmrk activity.[11,20]

In this study we continue our drug discovery efforts with Pfmrk by developing a 3D-QSAR pharmacophore model for inhibitor activity and identify potential inhibitors with the pharmacophore as a template for searching the WRAIR in-house 3D chemical databases by adopting the CATALYST procedures.[21,22]

Results

We developed a 3D-QSAR pharmacophore model for kinase inhibitory activity from a training set of 15 structurally diverse kinase inhibitors (Chart1). These compounds display a broad range of inhibitory activity against Pfmrk with experimental IC_{50} values ranging from 0.13 μM to 1100 μM (Table 1). On the basis of the structure−activity relationships within this set of compounds, pharmacophore models of Pfmrk inhibition were generated using the CATALYST procedure. The best model produced by CATALYST consisted of the spatial arrangement of four functional groups: two hydrogen-bond acceptors, one hydrophobic group, and one planar aromatic ring (Figure 1). The model shows an excellent correlation ($R = 0.9$) between experimental and predicted inhibitory activity of the kinase inhibitors of the training set. This pharmacophore was then used to estimate the Pfmrk inhibitory activity of a test set of 15 compounds (Table 2 and Chart 2) created from known kinase inhibitors that also showed inhibitory activity in our Pfmrk assay. The estimated IC_{50} values were compared with experimentally measured IC_{50} values in an effort to validate the pharmacophore model. The predicted and the experimental inhibitory activities correlate well ($R = 0.7$) despite most of the compounds in the set being CDK2 specific inhibitors. On the basis of the success of the cross-validation, the pharmacophore was used in an automated multiconformer 3D database search of the WR-CIS to identify new Pfmrk inhibitors.[23]

The CATALYST procedure resulted in the generation of 10 alternative pharmacophores describing the Pfmrk inhibitory activity of the training set compounds (see Experimental Section). These pharmacophore models were then evaluated by using them to estimate the inhibitory activity of the training set compounds. The

Table 1. Estimated and Experimentally Determined Activity Values of the Compounds in the Training Set

training set (compd no.)	compound name	IC_{50} (μM) exptl	est	error[a]
1	2-amino-2-methyl-1-(1-methyl-1*H*-indol-3-yl)propan-1-one hydrochloride	46.2	130.0	2.7
2	5-nitro-1*H*-indole-2,3-dione	5.9	5.3	−1.1
3	4-aza-8-nitroindolo[2,1-*b*]-quinazoline-6,12-dione	0.13	0.23	1.8
4	olomoucine	1100	69.0	−16.0
5	chloroquine	150.0	93.0	−1.6
6	mefloquine	12.0	21.0	1.8
7	4-(2,4-dihydroxyphenylazo)-3-hydroxy-naphthalene-1-sulfonic acid	11.0	30.0	2.7
8	2-hydrazino-3-(1*H*-indol-3-yl)-propionic acid	182.0	100.0	−1.8
9	3-(2-oxo-2-phenylethylidene)-1,3-dihydroindol-2-one	4.0	3.7	−1.1
10	5-bromo-3-(2-oxo-2-phenyl-ethylidene)-1,3-dihydroindol-2-one	3.1	2.9	−1.1
11	5,7-dimethyl-3-(2-oxo-2-phenyl-ethylidene)-1,3-dihydroindol-2-one	3.6	3.4	−1.1
12	5-bromo-3-(2-oxo-2-*p*-tolyl ethylidene)-1,3-dihydroindol-2-one	2.9	2.7	−1.1
13	3-[2-(4-bromophenyl)-2-oxo-ethylidene]-1-methyl-1,3-dihydroindol-2-one	29.0	78.0	2.7
14	3-(2-hydroxybenzylidene)-5-nitro-1,3-dihydroindol-2-one	35.0	44.0	1.2
15	5-methoxy-3-(4-oxo-2-thioxo-thiazolidin-5-ylidene)-1,3-dihydroindol-2-one	17.1	11.0	−1.5

[a] Values in the error column represent the ratio of estimated activity to experimental activity, or its negative inverse if the ratio is less than 1.

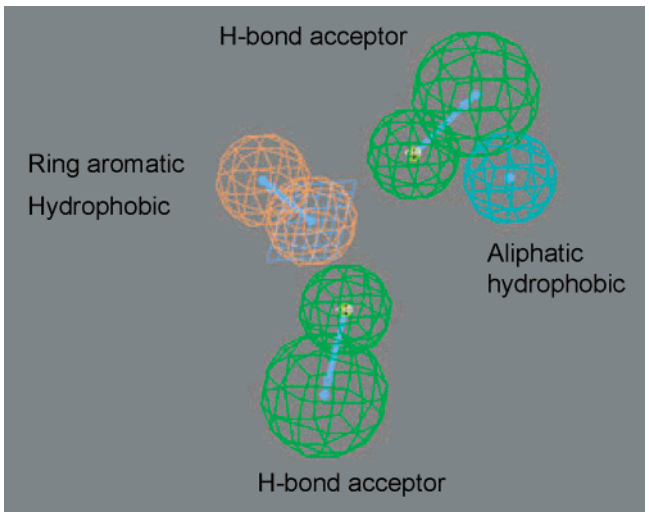

Figure 1. Pharmacophore for Pfmrk inhibitory activity.

correlation between the estimated and experimental values ranges between 0.9 and 0.7, and the RMS values range between 0.8 and 1.3. The statistical significance of the pharmacophores (hypotheses) falls within the recommended range of values in CATALYST (see *.log file in the Supporting Information). The difference between the fixed and the null cost is found to be 68 bits, indicating the robustness of the correlation. The cost difference between the first and the tenth hypothesis is 9.5 bits, closer to the fixed costs than the null costs. However, since the cost between the first and the tenth hypothesis is 9.5 bits and the difference of costs between these hypotheses and the null hypothesis ranges from 62.5 to 53 bits, it could be expected that

Table 2. Estimated and Experimentally Determined Activity Values of the Compounds in the Test Set

test set (compd no.)	compound name	IC_{50} (μM) exptl	est	error[a]
16	indirubin-3-monoxime {1*H*,1′*H*-[2,3′]bisindolylidene-3,2′-dione 3-oxime}	30.0	1.9	−15.0
17	alsterpaullone {9-nitro-5,12-dihydro-7*H*-benzo[2,3]azepino[4,5-*b*]indol-6-one}	51.0	12.0	−4.4
18	myricetin {3,5,7-trihydroxy-2-(3,4,5-tri-hydroxyphenyl)chromen-4-one}	157.0	25.0	−6.3
19	apigenin {5,7-dihydroxy-2-(4-hydroxy-phenyl)chromen-4-one}	7.0	5.3	−1.3
20	staurosporine	4.0	1.7	−2.4
21	bisindolylmaleimide 1 {3-[1-(3-dimethylaminopropyl)-1*H*-indol-3-yl]-4-(1*H*-indol-3-yl)-pyrrole-2,5-dione}	24.0	6.0	−4.0
22	NSU-45 {3-[3-(2-hydroxyethoxy)phenyl]-1*H*-quinolin-2-one}	18.0	8.3	−2.2
23	purvalanol A	26.0	3.1	−8.4
24	kenpaullone {9-bromo-5,12-dihydro-7*H*-benzo[2,3]azepino[4,5-*b*]indol-6-one}	15.0	43.0	2.9
25	5-(5-fluoro-2-oxo-1,2-dihydroindol-3-ylidene)thiazolidine-2,4-dione	30.0	6.7	−4.5
26	{2-chloro-*N*-(4-chlorobenzo-thiazol-2-yl)acetamide}	38.0	3.5	−11.0
27	{5-methyl-4-nitro-3-phenyl-1*H*-pyrazole}	394.0	220.0	−1.8
28	3-(4-trifluoromethylbenzylidene)-1,3-dihydroindol-2-one	138.0	17.0	−8.1
29	{5-bromo-3-[2-(4-fluorophenyl)-2-oxoethylidene]-1,3-dihydro-indol-2-one}	1.4	2.0	1.4
30	genistein {5,7-dihydroxy-3-(4-hydroxy-phenyl)chromen-4-one}	93.0	9.0	9.8

[a] Values in the error column represent the ratio of estimated activity toexperimental activity, or its negative inverse if the ratio is less than 1.

for all these hypotheses, there is a 78−92% chance of representing a true correlation in the data. All these calculated cost differences were found to be well within the acceptable limits recommended in the cost analysis of the CATALYST procedure.[22] The best pharmacophore model is characterized by two hydrogen bond acceptor functions, one aliphatic hydrophobic function, and one aromatic ring hydrophobic function (Figure 1) and is also statistically the most relevant model. The estimated activity values along with the experimental IC_{50} values for Pfmrk inhibition are presented in Table 1. A plot of the experimentally determined IC_{50} values versus the calculated activities demonstrates a strong correlation ($R = 0.9$) within the range of uncertainty 3, indicating a good predictive power of the model (Figure 2). The most potent compound in the training set, **3**, maps well to the functional features of the pharmacophore, whereas the least potent member of the series, **4**, maps poorly with the pharmacophore (Figure 3a,b). Inspection of Figure 3b clearly shows that **4** (olomoucine) fails to map the second hydrogen bond acceptor feature of the pharmacophore. Thus, it appears that the second hydrogen bond acceptor feature may be a specific requirement for binding to Pfmrk.

To cross-validate the pharmacophore, a set of 15 compounds was selected as a test set (Chart 2). These compounds are inhibitors of protein kinases and were assayed for Pfmrk inhibitory activity (Table 2).[19] Estimated activities were calculated by scoring the phar-

Chart 2

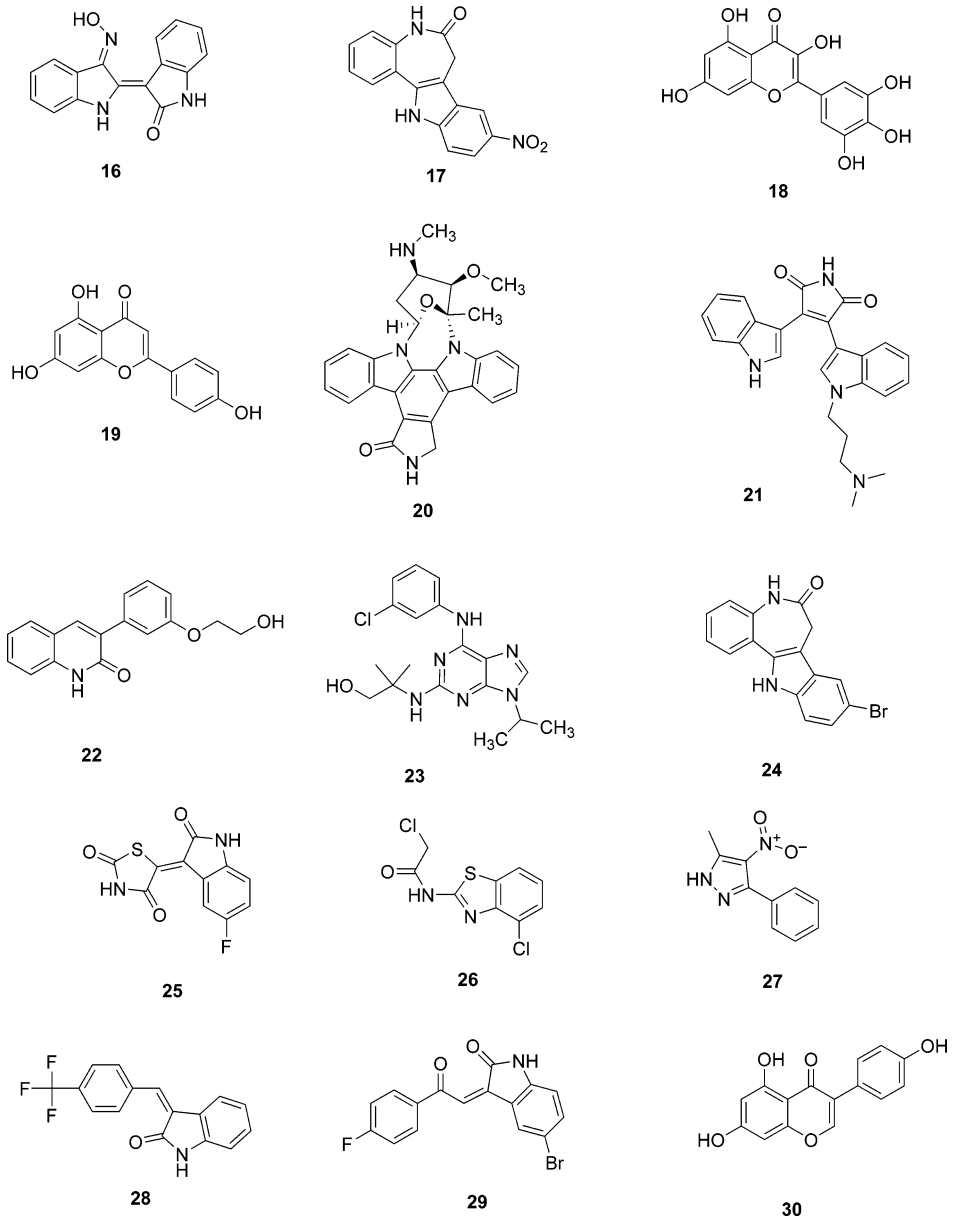

macophore model on the test set and comparing with the experimental IC_{50} values. The overall correlation between the estimated and experimental activities was 0.7, highlighting the predictive quality of the pharmacophore model. On average, the model-based estimated activities were slightly under predicted activities (negative error in Table 2) when compared with the experimental activities. The mapping of the pharmacophore on a few compounds of the test set is presented in Figure 4: **16** (Figure 4a), **20** (Figure 4b), **24** (Figure 4c), and **27** (Figure 4d).

We used the pharmacophore model template to conduct an in silico screen of our multiconformer 3D CIS chemical database at the Walter Reed Army Institute of Research. This screen evaluated the goodness of fit between the compounds in the chemical database and the pharmacophore model. The database search algorithm in CATALYST accounts for molecular flexibility of the compounds by considering each compound as an ensemble of conformers. The CIS database has approximately 290000 compounds.[23] For each compound, multiple conformations were generated (using the catDB utility algorithm of CATALYST) and conformational energies were assigned with respect to an energy-minimized structure. Through repeated refinement and search of this database in an iterative manner (see Compound Selection paragraph in Experimental Section), we were able to identify and shortlist 16 compounds with estimated activities below 25 μM (Chart 3**)** in our Pfmrk assay. The experimental IC_{50} values together with their predicted activities and conformational energy costs and the fit score (see Experimental Section for details) when mapped on the pharmacophore are shown in Table 3.

Discussion

The pharmacophore model developed in this project is composed of only four chemical functions localized in space, yet it proved to be an efficient predictive tool. We found that the pharmacophore was instrumental in conducting a targeted assay of the 290000 compounds in the WR-CIS. Even though we have developed an

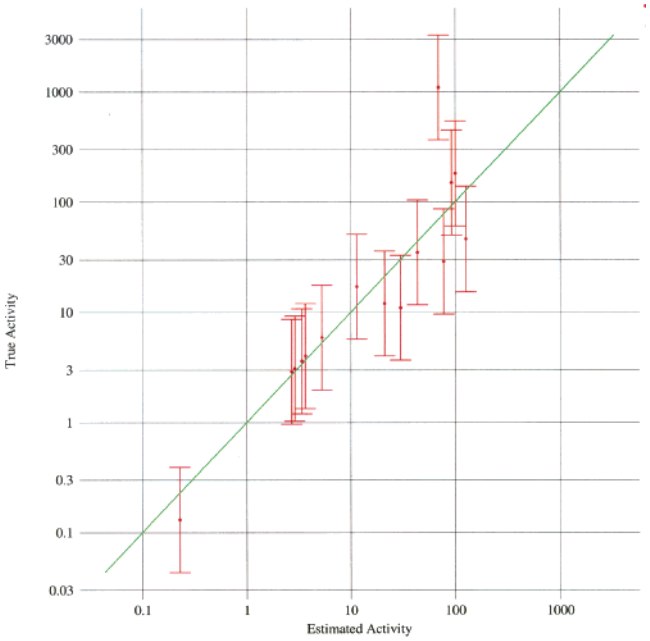

Figure 2. Correlation ($R = 0.9$) line displaying the observed versus estimated IC_{50} values (μM) of the training set by using the statistically most significant pharmacophore derived from the experimental Pfmrk activities. (*Y*-axis shows the experimental activity, and *X*-axis represents the predicted activity.)

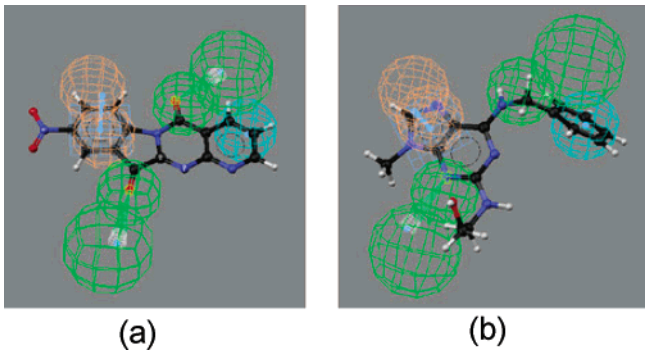

Figure 3. Mapping of (a) the most potent analogue, **3**, and (b) the least potent analogue, **4**, onto the pharmacophore model.

automated, plate-based in vitro assay for Pfmrk activity, time and resource costs prohibited an exhaustive search of the entire chemical database. Thus, it was essential to our effort to develop a predictive tool that would allow us to identify a limited number of compounds for in vitro screening. The pharmacophore was developed for this purpose. Before database screening, however, the model was validated on a test set of 15 compounds known to inhibit human CDK2 (Table 2 and Chart 2). The Pfmrk inhibitory activities that were estimated using the model were well correlated ($R = 0.7$) to the experimentally measured activities (Table 2**)**.

The pharmacophore model was then used to screen the WRAIR chemical database. Sixteen compounds with predicted inhibitory activity below 25 μM were selected and tested in the in vitro Pfmrk assay. All of these compounds (Chart 3) displayed Pfmrk inhibitory activity below 100 μM, demonstrating the predictive value of the pharmacophore (Table 3). Eight of these compounds, **31**, **36**, **39**, **40**, **42**, **43**, **44**, and **46**, map well to the four features of the pharmacophore, whereas the other eight map well to only three features. Figure 5a,b shows **31**

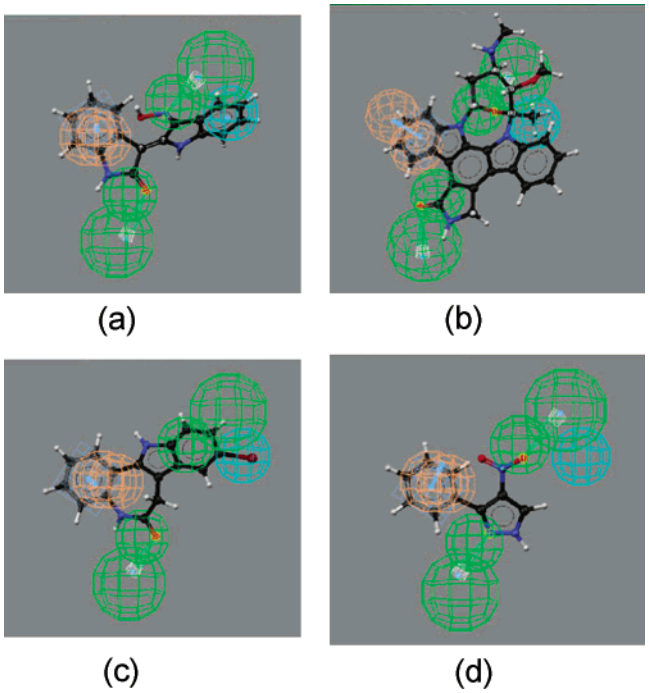

Figure 4. Mapping of compounds from the test set onto the pharmacophore: (a) **16**, (b) **20**, (c) **24**, and (d) **27**.

Table 3. Sixteen Compounds Discovered Using the Pharmacophore through Multiconformer 3D CIS Database Searches along with Their Experimental and Predicted Activities

compd no.	compd name	fit score	coformational energy (kcal/mol)	activity (μM) est	activity (μM) exptl
31	4-aza-9-chloroindolo[2,1-*b*]-quinazoline-6,12-dione	7.1	0.0	0.2	3.5
32	2-{(2-hydroxyethyl)[5-(4-methoxyphenyl)[1,3,4]oxadiazol-2-yl]amino}ethanol	5.9	11.3	2.7	35.8
33	3-oxo-1-phenyl-1,3-dihydroisobenzofuran-1-yl)thiourea	5.0	13.3	25.0	70.0
34	2-chloro-*N*-(4-chlorobenzothiazol-2-yl)acetamide	5.3	2.4	13.0	38.3
35	1-(3-nitrophenyl)-3-phenylpropenone	6.5	2.6	0.8	10.0
36	5-chloro-4-nitrothiophene-2-sulfonic acid (4-trifluoromethylphenyl)-amide	7.5	4.8	0.1	2.5
37	1-(4-nitrophenyl)-3- pyridin-2-ylpropenone	6.1	2.5	2.0	18.0
38	3,9,11-trichloro-5,6-dihydrobenzo[*c*]acridine-7-carbonyl chloride	6.0	0.0	2.2	25.0
39	(4-chlorophenyl)-[3-(4-chlorophenyl)-2,4-dioxooxazolidin-5-ylidene]acetonitrile	6.5	0.0	0.8	14.0
40	ethyl 2-chloro-5-nitrobenzoate	7.4	2.1	1.0	87.0
41	2-pyridin-2-ylmethylene-3,4-dihydro-2*H*-naphthalen-1-one	5.1	0.0	18.0	17.0
42	ethyl 2-(4-nitrobenzoyl)-3-pyridin-2-ylacrylate	6.9	7.0	0.3	61.0
43	1-(2,4-dichlorobenzoyl)-3-(2-hydroxy-5-nitrophenyl)-thiourea	7.1	0.0	0.2	10.0
44	*N*-(4-chloro-2-methylphenyl)-3-nitrobenzamide	7.8	0.0	0.04	69.0
45	*N*-[4-(3-phenylacryloyl)-phenyl]acetamide	6.0	2.4	2.7	17.0
46	4-aza-8-fluoroindolo[2,1-*b*]-quinazoline-6,12-dione	7.0	0.0	0.2	4.7

and **36** mapped to all four features of the model while Figure 5c shows **33**, which maps well to three features, but is missing a hydrophobic feature, and Figure 5d

Chart 3

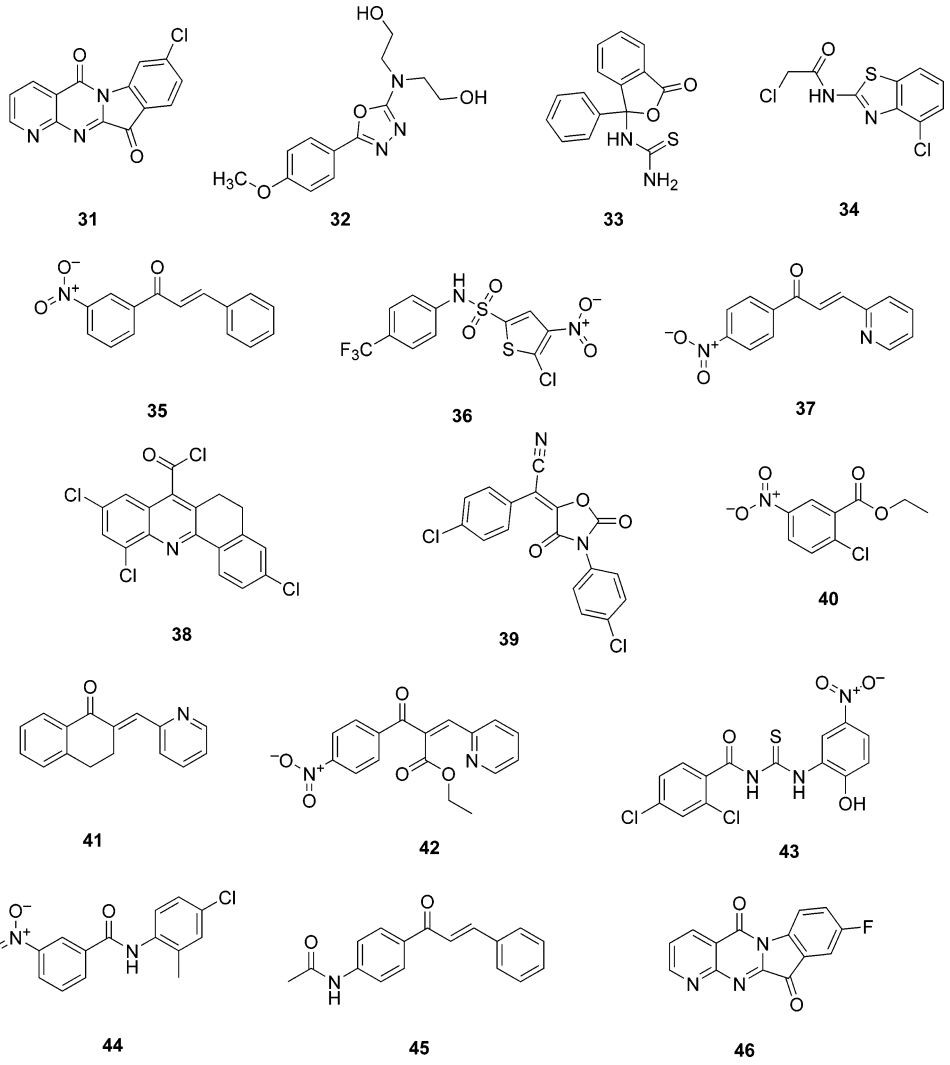

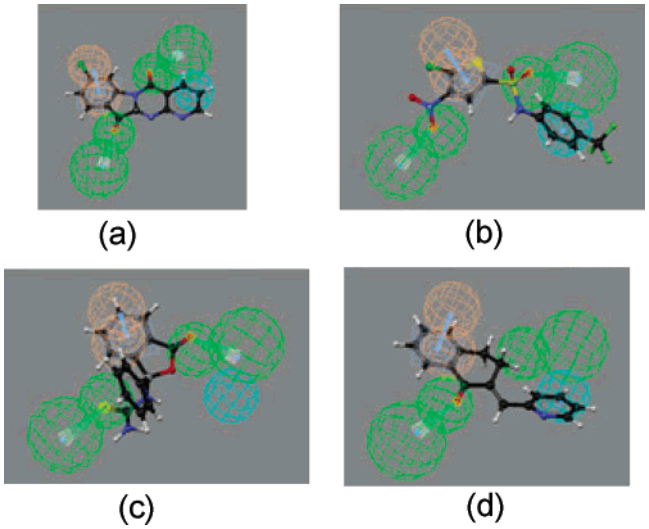

Figure 5. Mapping of the Pfmrk inhibitors discovered through database searches onto the pharmacophore: (a) **31**, (b) **36**, (c) **33**, and (d) **41**.

shows **41** mapping well to three features, but missing one H-bond acceptor.

The group of compounds that match all four features of the model includes the best inhibitors (**31**, **36**, and **46**), but this group also includes compounds with the worst inhibitory activity (**37**, **40**, and **44**). This latter group shares a structural feature: a nitrophenyl group. The pharmacophore model contains a hydrogen-bond acceptor 3.4 Å from the centroid of a planar aromatic ring. These features map very well to a nitrophenyl group both in distance and in orientation, perhaps explaining why six of the sixteen compounds identified by the screen contain this moiety. As discussed below, nitrophenyl groups may not be well tolerated in the Pfmrk active site despite the fact that they map well to the pharmacophore model. The six compounds containing nitrophenyl groups have an average estimated activity of 0.7 μM while the average experimental value is 61-fold higher (43 μM). For the remaining 10 compounds, the average estimated activity and average experimental activity differ by less than 4-fold.

A wealth of structural information exists for CDKs. Crystal structures of human CDK2 account for most of this information: over 75 structures have been determined of this enzyme. Structures of human CDK2 have been determined with bound cyclin, bound substrate (ATP), and bound inhibitors, as well as with phosphorylation of key regulatory sites on the kinase. Combined, these structures provide a basis for understanding the activity, regulation, and inhibition of CDKs.[24−27] Structures of CDK2 with bound small molecule inhibitors are

particularly useful for interpreting the results of our pharmacophore-based screen. In most of these structures (44 of 48 structures examined), the main chain amide group of Leu83 forms a hydrogen bond with an acceptor group on the inhibitor.[26,28] This hydrogen bond mimics the one formed between the amide of Leu83 and the adenine N1 when ATP is bound in the CDK2 active site. A homology model of Pfmrk, based on the structures of CDK2, indicates that Met94 occupies this position in Pfmrk and that this hydrogen bond is important for ATP and inhibitor binding to Pfmrk.[11,19] Recent structures of a malaria CDK (PfPK5) show that bound inhibitors also form this hydrogen bond to the CDK active site.[10] Thus, analysis of the Pfmrk homology model combined with the X-ray crystal structures of CDK/inhibitor complexes highlights the importance of a hydrogen-bond acceptor in the inhibitor that can form a hydrogen bond with the amide group of residue 94 (Pfmrk numbering).

The pharmacophore model contains two hydrogen bond acceptor features, one of which may represent the interaction with Met94 in the Pfmrk active site. As discussed above, one of these hydrogen-bond acceptors is 3.4 Å from the centroid of the aromatic ring feature in the pharmacophore. It is these two pharmacophore features that appear to account for the important binding properties of the adenine base of substrate ATP. These features also map well to all of the compounds identified in our screen that demonstrate potent Pfmrk inhibition. It has been reported that there are some areas of the ATP binding pocket that are occupied by flat aromatic rings of CDK2 inhibitors, such as roscovitine, flavopiridol, and staurosporin.[29,30] These areas in CDK2 are surrounded by hydrophobic amino acid residues, Ile10, Val18, Ala31, Val64, Phe80, Phe82, Leu134, and Ala144 in a narrow cavity. This cavity is occupied by aromatic rings in all structurally characterized interactions between CDK2 and small molecule inhibitors. Amino acid alignment between Pfmrk and CDK2 identify a similar hydrophobic pocket within the active site of Pfmrk which consists of Leu16, Val24, Ala37, Met75, Met91, Ile93, Phe143, and Ala153.[13] The structures of PfPK5 also show that the aromatic rings of the bound inhibitors are bound in a hydrophobic pocket lined with these residues.[10] Thus, the aromatic ring and hydrogen bond acceptor features of the pharmacophore may represent general requirements for inhibitor and ATP binding to CDKs.

The Pfmrk pharmacophore contains two additional features: a second hydrogen-bond acceptor and a hydrophobic group. These features are difficult to rationalize on the basis of the X-ray crystal structures of CDK2 and PfPK5 and the binding modes of inhibitors found in these structures. These features may be requirements for specific binding to Pfmrk rather than general features shared by CDK inhibitors. Inhibitor selectivity is a key concern in drug discovery projects that target cyclin-dependent kinases. The malaria parasite appears to have several CDKs, and humans have at least nine more. Inhibitor specificity can rely on relatively subtle differences between CDK active sites. A good example is the selectivity between human CDK4 and CDK2. Recent efforts to target CDK4 used a CDK2 variant that contained three active site amino acid substitutions.[12,24,31] The mutant CDK2 displayed activity and inhibitor selectivity similar to that of CDK4. Binding requirements specific to Pfmrk must be encoded in the pharmacophore since it is able to predict Pfmrk inhibition ($R = 0.7$) when presented with a series of potent CDK2 inhibitors (Table 2). Specificity is an important quality of the pharmacophore model since most CDK inhibitors are poor inhibitors of Pfmrk activity. Recent work on oxindole-based inhibitors of Pfmrk suggests that hydrophobic active site residues may be responsible for the selectivity of these Pfmrk inhibitors.[11] In particular, three residues (Leu16, Tyr96, and Phe143) are unique to Pfmrk and could create additional hydrophobic interfaces not present in PfPK5 and CDK2. The hydrophobic feature (nonaromatic) of the pharmacophore may be targeting these unique aspects of the Pfmrk active site.

The pharmacophore model developed by using the CATALYST procedures in this study proved to have useful predictive value. However, the pharmacophore model has limitations due to the simplicity of the model. A good example is the selection of compounds containing nitrophenyl groups discussed above. The nitrophenyl group maps very well to two features in the pharmacophore (hydrogen-bond acceptor 3.4 Å from the centroid of a planar aromatic ring); however, compounds containing this group are poor inhibitors of Pfmrk. As discussed above, these pharmacophore features probably map to the binding site of the purine ring of substrate ATP. Purine analogue inhibitors bind well, but charged groups like nitrophenyl do not. No CDK/inhibitor complexes have been structurally determined with a charged group in this region of the active site. The pharmacophore model does not contain this level of discrimination and overpredicts the binding affinity of some compounds.

Conclusion

Our in silico pharmacophore model accounts for Pfmrk-specific inhibitory activity and allowed us to identify several potent Pfmrk inhibitors through 3D database searches. The model was developed solely from compound structure−activity relationships, yet it is very consistent with what is known from nearly 50 X-ray crystal structures of CDKs with bound inhibitors. The pharmacophore model contains features that appear to be shared by a wide range of general CDK inhibitors, as well as features that appear to be Pfmrk-specific. Despite the complexity of *P. falciparum* cyclin-dependent kinase activity, the predicted Pfmrk inhibition from our pharmacophore model is robust (Table 3). We are currently involved in the design of highly selective Pfmrk inhibitors based on this binding mode and structure−function information about the differences between Pfmrk and other kinases.

Experimental Section

Kinase Drug Screen. Pfmrk, PfPK5, and Pfcyc-1 were expressed and purified from *Escherichia coli* as GST tagged (Pfcyc-1) or 6xHIS tagged (Pfmrk, PfPK5) as previously reported.[19,32] Plasmodial CDKs were screened in a filter bottom microtiter plate assay to identify selective inhibitors as previously described. Briefly, 3.0 μg of kinase was assayed in a 50 μL reaction containing kinase buffer (40 mM Hepes pH 7.5, 30 mM $MnCl_2$, and 2.0 mM DTT) supplemented with 2.0 μg of

Pfcyc-1 and 5.0 μg of carboxy-terminal domain of RNA polymerase II (CTD). Kinases were preincubated for 5 min at 30 °C with kinase reaction buffer and various concentrations of compounds to facilitate binding of compounds to the kinases. Following preincubation, the reaction was started by the addition of 2.0 μCi of [γ-^{32}P]ATP, 3000 Ci/mmol (Amersham), and 12.5 μM adenosine triphosphate (ATP tris salt). The activity was then assayed at 30 °C for 35 min. Plates were washed on a vacuum manifold (Whatman) with 5% phosphoric acid. Scintillation fluid was added to each well and activity measured in a Topcount microtiter plate scintillation counter (Packard). Each reaction was assayed in triplicate and counts per minute averaged with a variation of less than 5%. Selected inhibitors were assayed across a broad range of concentration to calculate IC_{50} values.

Procedure for Generation of the 3D QSAR Model. The three-dimensional pharmacophore was developed using the CATALYST 4.7 software (Accelrys Inc., San Diego, CA).[22] This is an integrated commercially available software package that generates pharmacophores, commonly referred to as hypotheses. It enables the use of structure and activity data for a set of lead compounds to create a hypothesis, thus characterizing the activity of the lead set. At the heart of the software is the HypoGen algorithm that allows identification of hypotheses that are common to the "active" molecules in the training set but at the same time not present in the "inactives".[33] Structures of 15 kinase inhibitors of the training set were either built from the fragments or imported into CATALYST from other directories and energy minimized to the closest local minimum using the generalized CHARMM-like force field as implemented in the program. The CATALYST model treats molecular structures as templates comprising chemical functions localized in space that will bind effectively with complementary functions on the respective binding proteins. The most relevant chemical features are extracted from a small set of compounds that cover a broad range of activity. Molecular flexibility is taken into account by considering each compound as an ensemble of conformers representing different accessible areas in 3D space. The "best searching procedure" was applied to select representative conformers within 20 kcal/mol from the global minimum.[34] The conformational model of the training set was used for hypothesis (pharmacophore) generation within CATALYST, which aims to identify the best 3-dimensional arrangement of chemical functions explaining the activity variations among the compounds in the training set. The automatic generation procedure using the HypoGen algorithm in CATALYST was adopted for generation of the hypotheses. In order to obtain a reliable model which adequately describes the interaction of ligands with high predictability, the method recommends a collection of 15−20 chemically diverse molecules with biological activity covering 4−5 orders of magnitude for the training set.

The pharmacophores/hypotheses are described by a set of functional features such as hydrophobic, hydrogen-bond donor, hydrogen-bond acceptor, and positively and negatively ionizable sites distributed over a 3D space. The hydrogen-bonding features are vectors, whereas all other functions are points. The statistical relevance of the obtained hypotheses is assessed on the basis of their cost relative to the null hypothesis and their correlation coefficient.

Pharmacophore generation was carried out with the 15 kinase inhibitors (Chart 1) by setting the default parameters in the automatic generation procedure in CATALYST such as function weight 0.302, mapping coefficient 0, resolution 297 pm, and activity uncertainty 3. An uncertainty Δ in the CATALYST paradigm indicates an activity value lying somewhere in the interval from "activity divided by Δ" to "activity multiplied by Δ". Hypotheses approximating the pharmacophore of the kinase inhibitors are described as a set of aromatic hydrophobic, hydrogen-bond acceptor, hydrogen bond acceptor lipid, positively and negatively ionizable sites distributed within a 3D space. The statistical relevance of various generated hypotheses is assessed on the basis of the cost relative to the null hypothesis and the correlation coefficients. The hypotheses are then used to estimate the activities of the training set. These activities are derived from the best conformation generation mode of the conformers displaying the smallest root-mean-square (RMS) deviations when projected onto the hypothesis. HypoGen considers a pharmacophore that contain features with equal weights and tolerances. Each feature (e.g., hydrogen-bond acceptor, hydrogen-bond donor, hydrophobic, positive ionizable group, etc.) contributes equally to estimate the activity. Similarly, each chemical feature in the HypoGen pharmacophore requires a match to a corresponding ligand atom to be within the same distance (tolerance).[35] Thus, two parameters, such as the fit score and conformational energy costs, are crucial for estimation of predicted activity of the compounds. The method has been documented to perform better than a structure-based pharmacophore generation.[34−36]

The pharmacophore developed in the study was used as a template to search the in-house Chemical Information System (CIS) database and identify new Pfmrk inhibitors. The CIS database has over 290000 compounds, and the structure of each of these compounds was transformed into all conformations ranging from 0 to 20 kcal/mol and stored into a multiconformer form CIS database by using the catDB utility program of the software. The catDB format allows a molecule to be represented by a limited set of conformations, thereby permitting conformational flexibility to be included during the search of the database.

Compound Selection. The pharmacophore mapped on one of the potent inhibitors was converted into a shape-based 3D template to account for the steric factors associated with the binding. This template was used to search of the chemical inventory system at Walter Reed Army Institute of Research (CIS-WRAIR). Each compound in the CIS was converted into 3D multiconformations with an energy range of 0−20 kcal/mol using the catDB algorithm of CATALYST and stored in an SGI Octane workstation. The down selection of the identified compounds was carried out by evaluating the in silico ADME/toxicity properties and choosing only those compounds that have favorable properties. ADME/toxicity evaluations were carried out by using Cerius[2] and TOPKAT[37] methodology as implemented in these software. The overall procedure of compound identification and selection was carried out in an iterative manner by generating several shape-based pharmacophore templates on a few other potent Pfmrk inhibitors. Ultimately, we were able to shortlist 16 compounds to be assayed as potential inhibitors of plasmodial CDKs.

Supporting Information Available: Statistical significance of the reported pharmacophores with a table showing the details of the statistics. High-resolution mass spectral data analysis and chromatographic data of six representative compounds, provided to establish their homogeneity and purity criteria for the target compounds. This material is available free of charge via the Internet at http://pubs.acs.org.

References

(1) Breman, J. G. The ears of the hippopotamus: manifestations, determinants, and estimates of the malaria burden. *Am. J. Trop. Med. Hyg.* **2001**, *64*, 1−11.
(2) Winstanley, P. A.; Ward, S. A.; Snow, R. W. Clinical status and implications of antimalarial drug resistance. *Microbes Infect.* **2002**, *4*, 157−164.
(3) Meijer, L.; Leclerc, S.; Leost, M. Properties and potential-applications of chemical inhibitors of cyclin-dependent kinases. *Pharmacol. Ther.* **1999**, *82*, 279−284.
(4) Fischer, P. M.; Lane, D. P. Inhibitors of Cyclin-Dependent Kinases as Anti-Cancer Therapeutics. *Curr. Med. Chem.* **2000**, *7*, 1213−1245 [Record as supplied by publisher].
(5) O'Hare, M.; Wang, F.; Park, D. S. Cyclin-dependent kinases as potential targets to improve stroke outcome. *Pharmacol. Ther.* **2002**, *93*, 135−143.
(6) Monaco, E. A., 3rd; Vallano, M. L. Cyclin-dependent kinase inhibitors: cancer killers to neuronal guardians. *Curr. Med. Chem.* **2003**, *10*, 367−379.
(7) Ivorra, C.; Samyn, H.; Edo, M. D.; Castro, C.; Sanz-Gonzalez, S. M.; et al. Inhibiting cyclin-dependent kinase/cyclin activity for the treatment of cancer and cardiovascular disease. *Curr. Pharm. Biotechnol.* **2003**, *4*, 21−37.

(8) Knockaert, M.; Greengard, P.; Meijer, L. Pharmacological inhibitors of cyclin-dependent kinases. *Trends Pharmacol. Sci.* **2002**, *23*, 417−425.
(9) Keenan, S. M.; Welsh, W. J. Characteristics of the Plasmodium falciparum PK5 ATP-binding site: implications for the design of novel antimalarial agents. *J. Mol. Graphics Modell.* **2004**, *22*, 241−247.
(10) Holton, S.; Merckx, A.; Burgess, D.; Doerig, C.; Noble, M.; et al. Structures of P. falciparum PfPK5 test the CDK regulation paradigm and suggest mechanisms of small molecule inhibition. *Structure (Camb)* **2003**, *11*, 1329−1337.
(11) Woodard, C. L.; Li, Z.; Kathcart, A. K.; Terrell, J.; Gerena, L.; et al. Oxindole-based compounds are selective inhibitors of *Plasmodium falciparum* cyclin dependent protein kinases. *J. Med. Chem* **2003**, *46*, 3877−3882.
(12) Ikuta, M.; Kamata, K.; Fukasawa, K.; Honma, T.; Machida, T.; et al. Crystallographic approach to identification of cyclin-dependent kinase 4 (CDK4)-specific inhibitors by using CDK4 mimic CDK2 protein. *J. Biol. Chem.* **2001**, *276*, 27548−27554.
(13) Waters, N. C.; Geyer, J. A. Cyclin-dependent protein kinases as therapeutic drug targets for antimalarial drug development. *Expert Opin. Ther. Targets* **2003**, *7*, 7−17.
(14) Doerig, C.; Endicott, J.; Chakrabarti, D. Cyclin-dependent kinase homologues of Plasmodium falciparum. *Int. J. Parasitol.* **2002**, *32*, 1575−1585.
(15) Ross-Macdonald, P. B.; Graeser, R.; Kappes, B.; Franklin, R.; Williamson, D. H. Isolation and expression of a gene specifying a cdc2-like protein kinase from the human malaria parasite Plasmodium falciparum. *Eur. J. Biochem.* **1994**, *220*, 693−701.
(16) Graeser, R.; Wernli, B.; Franklin, R. M.; Kappes, B. Plasmodium falciparum protein kinase 5 and the malarial nuclear division cycles. *Mol. Biochem. Parasitol.* **1996**, *82*, 37−49.
(17) Harmse, L.; van Zyl, R.; Gray, N.; Schultz, P.; Leclerc, S.; et al. Structure-activity relationships and inhibitory effects of various purine derivatives on the in vitro growth of Plasmodium falciparum. *Biochem. Pharmacol.* **2001**, *62*, 341−348.
(18) Li, J. L.; Robson, K. J.; Chen, J. L.; Targett, G. A.; Baker, D. A. Pfmrk, a MO15-related protein kinase from Plasmodium falciparum. Gene cloning, sequence, stage-specific expression and chromosome localization. *Eur. J. Biochem.* **1996**, *241*, 805−813.
(19) Waters, N. C.; Woodard, C. L.; Prigge, S. T. Cyclin H activation and drug susceptibility of the Pfmrk cyclin dependent protein kinase from Plasmodium falciparum. *Mol. Biochem. Parasitol.* **2000**, *107*, 45−55.
(20) Xiao, Z.; Waters, N. C.; Woodard, C. L.; Li, Z.; Li, P. K. Design and synthesis of Pfmrk inhibitors as potential antimalarial agents. *Bioorg. Med. Chem. Lett.* **2001**, *11*, 2875−2878.
(21) *CATALYST*, 4.7 ed.; Accelrys: San Diego, CA.
(22) Kurogi, Y.; Guner, O. F. Pharmacophore modeling and three-dimensional database searching for drug design using catalyst. *Curr. Med. Chem.* **2001**, *8*, 1035−1055.
(23) Chemical Information System; Division of Experimental Therapeutics, Walter Reed Army Institute of Research, Silver Spring, MD.
(24) Honma, T.; Hayashi, K.; Aoyama, T.; Hashimoto, N.; Machida, T.; et al. Structure-based generation of a new class of potent Cdk4 inhibitors: new de novo design strategy and library design. *J. Med. Chem.* **2001**, *44*, 4615−4627.
(25) De Bondt, H. L.; Rosenblatt, J.; Jancarik, J.; Jones, H. D.; Morgan, D. O.; et al. Crystal structure of cyclin-dependent kinase 2. *Nature* **1993**, *363*, 595−602.
(26) Hardcastle, I. R.; Golding, B. T.; Griffin, R. J. Designing inhibitors of cyclin-dependent kinases. *Annu. Rev. Pharmacol. Toxicol.* **2002**, *42*, 325−348.
(27) Brown, N. R.; Noble, M. E.; Lawrie, A. M.; Morris, M. C.; Tunnah, P.; et al. Effects of phosphorylation of threonine 160 on cyclin-dependent kinase 2 structure and activity. *J. Biol. Chem.* **1999**, *274*, 8746−8756.
(28) Noble, M. E.; Endicott, J. A. Chemical inhibitors of cyclin-dependent kinases: insights into design from X-ray crystallographic studies. *Pharmacol. Ther.* **1999**, *82*, 269−278.
(29) De Azevedo, W. F.; Leclerc, S.; Meijer, L.; Havlicek, L.; Strnad, M.; et al. Inhibition of cyclin-dependent kinases by purine analogues: crystal structure of human cdk2 complexed with roscovitine. *Eur J. Biochem.* **1997**, *243*, 518−526.
(30) De Azevedo, W. F., Jr.; Mueller-Dieckmann, H. J.; Schulze-Gahmen, U.; Worland, P. J.; Sausville, E.; et al. Structural basis for specificity and potency of a flavonoid inhibitor of human CDK2, a cell cycle kinase. *Proc. Natl. Acad. Sci. U.S.A.* **1996**, *93*, 2735−2740.
(31) Honma, T.; Yoshizumi, T.; Hashimoto, N.; Hayashi, K.; Kawanishi, N.; et al. A novel approach for the development of selective Cdk4 inhibitors: library design based on locations of Cdk4 specific amino acid residues. *J. Med. Chem.* **2001**, *44*, 4628−4640.
(32) Le Roch, K.; Sestier, C.; Dorin, D.; Waters, N.; Kappes, B.; et al. Activation of a Plasmodium falciparum cdc2-related kinase by heterologous p25 and cyclin H. Functional characterization of a P. falciparum cyclin homologue. *J. Biol. Chem.* **2000**, *275*, 8952−8958.
(33) Gunner, O. A. *Pharmacophore, perception, development, and use in drug design*; University International Line: San Diego, 2000; pp 17−20.
(34) Grigorov, M.; Weber, J.; Tronchet, J. M.; Jefford, C. W.; Milhous, W. K.; et al. A QSAR study of the antimalarial activity of some synthetic 1,2,4-trioxanes. *J. Chem. Inf. Comput. Sci.* **1997**, *37*, 124−130.
(35) Greenidge, P. A.; Weiser, J. A comparison of methods for pharmacophore generation with the catalyst software and their use for 3D-QSAR: application to a set of 4-aminopyridine thrombin inhibitors. *Mini-Rev. Med. Chem.* **2001**, *1*, 79−87.
(36) Bhattacharjee, A. K.; Hartell, M. G.; Nichols, D. A.; Hicks, R. P.; Stanton, B.; et al. Structure-activity relationship study of antimalarial indolo [2,1-b]quinazoline-6,12-diones (tryptanthrins). Three-dimensional pharmacophore modeling and identification of new antimalarial candidates. *Eur. J. Med. Chem.* **2004**, *39*, 59−67.
(37) *Cerius2 and Topkat*; Accelrys Inc: San Diego, CA.

JM040108F